

The first indication of excess acoustic power in other stars with a frequency dependence similar to the Sun was reported by Brown et al. (1991) for the F5 star Procyon A (α CMi), in which the first unambiguous detection of solar-like oscillations was reported by Martić et al. (1999), confirmed later by Mosser et al. (2008). First (unconfirmed) detection of individual peaks in the acoustic power spectrum from high-precision time-resolved spectroscopic observations was published for the G5 star η Boo by Kjeldsen et al. (1995), but it was not before 2003 that an unambiguous confirmation was established by Carrier et al. (2003) and Kjeldsen et al. (2003). The location of stars in the Hertzsprung-Russell diagram, in

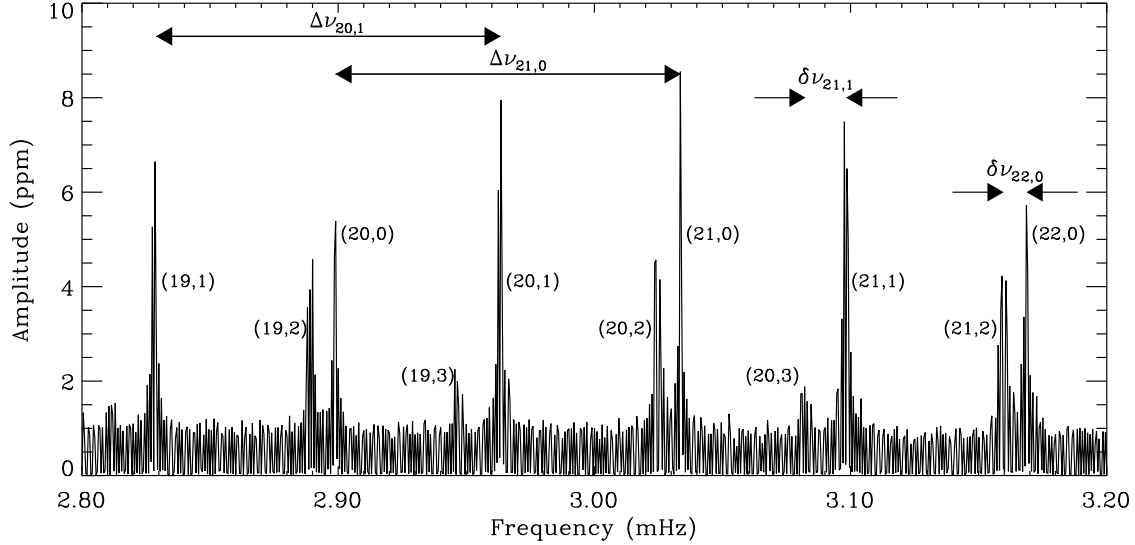


FIGURE 2. Small section of a solar acoustic power spectrum. The radial order n and spherical degree l are indicated in pairs of (n, l) for each mode. The large and small frequency separations, $\Delta\nu_{n,l}$ and $\delta\nu_{n,l}$ are in general functions of n and l and can be used to infer the mass and age of a star (adapted from Christensen-Dalsgaard 2001).

which solar-like oscillations have been detected until today, are indicated in Fig. 1, and a summary of such stars was presented recently by Bedding & Kjeldsen (2007).

SOLAR-LIKE OSCILLATION PROPERTIES

Only modes of low degree can be observed in distant stars, however, in general, the observed modes are of high radial order, which allows us to extract diagnostic properties of the frequencies $\nu_{n,l}$ with radial order n and spherical degree l for the asymptotic limit $n/l \rightarrow \infty$. The diagnostic properties of this type of mode have been studied extensively in the solar case. From asymptotic theory we find for the cyclic oscillation frequencies (Gough 1986, 1993; see also Tassoul 1980 and Vandakurov 1967)

$$\nu_{n,l} \simeq \left(n + \frac{l}{2} + \hat{\epsilon}\right) \nu_0 - \frac{AL^2 - B}{\nu_{n,l}} \nu_0^2 + O(\nu_0^4), \quad (1)$$

where

$$\nu_0 = \left[2 \int_0^R \frac{dr}{c}\right]^{-1} \quad (2)$$

is the inverse of twice the sound travel time between the centre and surface (R is surface radius), and

$$A = \frac{1}{4\pi^2 \nu_0} \left[\frac{c(R)}{R} - \int_0^R \frac{dc}{dr} \frac{dr}{r} \right]. \quad (3)$$

The frequency-dependent coefficient $\hat{\epsilon}$ is determined by the reflection properties of the surface layers, as is the small correction term B , and $L^2 = l(l+1)$. The value

of ν_0 can be estimated from taking the average (over n and l) of the so-called large frequency separation $\Delta\nu_{n,l} \equiv \nu_{n,l} - \nu_{n-1,l}$ between modes of like degree and consecutive order. The last two terms on the right-hand side of equation (1) lift the degeneracy between modes with the same value of $n + l/2$ and leads to the so-called small frequency separation $\delta\nu_{n,l} \equiv \nu_{n,l} - \nu_{n-1,l+2}$. One obtains a frequency structure in which modes of odd degree fall approximately halfway between modes of even degree, which is illustrated in Fig. 2 for a solar spectrum. The mean small frequency separation (averaged over n)

$$\langle \delta\nu_{n,l} \rangle = \langle \nu_{n,l} - \nu_{n-1,l+2} \rangle \simeq [2A(2l+3)] \frac{\nu_0^2}{\langle \nu_{n,l} \rangle} \quad (4)$$

is predominantly determined by the acoustic sound speed in the stellar core and hence is sensitive to the chemical composition there and consequently is an indicator for the stellar age (e.g., Gough 2001, Houdek & Gough 2008).

Seismic diagnostic

Acoustic modes depend predominantly on the sound speed in the stellar interior and consequently on the chemical composition. As the star evolves, the chemical composition will vary and consequently also the value of the small frequency separation $\delta\nu_{n,l}$. So does the mean large frequency separation (averaged over n and l)

$$\langle \Delta\nu \rangle = \langle \nu_{n,l} - \nu_{n-1,l} \rangle \simeq \nu_0 \propto (M/R^3)^{1/2} \quad (5)$$

mainly because of the increasing surface radius with time. A convenient way to demonstrate the dependence

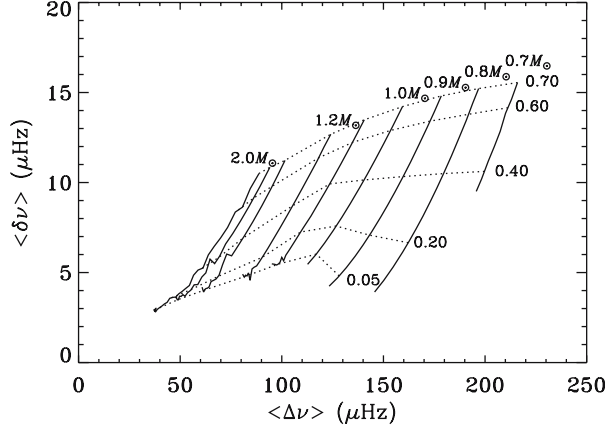


FIGURE 3. Stellar evolutionary tracks (solid curves, indicated by the stellar mass) and curves of constant central hydrogen abundance (dashed curves, indicated by the central hydrogen abundance by mass, X_c) in terms of the average large separation $\langle \Delta \nu \rangle$ and average small separation $\langle \delta \nu \rangle \equiv \langle \delta \nu_{n0} \rangle$ [c.f. equations (5) & (4)] (from Christensen-Dalsgaard 1993).

of the sound speed and radius on the effects of stellar evolution can be illustrated in a $(\langle \Delta \nu \rangle, \langle \delta \nu \rangle)$ diagram, depicted in Fig. 3.

Additional information of structural aspects of solar-like stars is obtained from the seismic signatures contained in $\Delta \nu_{n,l}$ and $\delta \nu_{n,l}$. Abrupt variation in the stratification of a star (relative to the scale of the inverse radial wavenumber of a seismic mode of oscillation), such as that resulting from the (smooth, albeit acoustically relatively abrupt) depression in the first adiabatic exponent $\gamma = (\partial \ln p / \partial \ln \rho)_s$ caused by the ionization of helium, where p , ρ and s are pressure, density and specific entropy, or from the sharp transition from radiative to convective heat transport at the base of the convection zone, induces small-amplitude oscillatory components (with respect to frequency) in the spacing of the cyclic eigenfrequencies $\nu_{n,l}$ of seismic oscillation and consequently also in $\Delta \nu_{n,l}$ and $\delta \nu_{n,l}$. We call such abrupt variations an acoustic glitch. One might hope that the variation of the sound speed c induced by helium ionization might enable one to determine from the low-degree eigenfrequencies a measure that is directly related to, perhaps even almost proportional to, the helium abundance, with little contamination from other properties of the structure of the star.

A convenient and easily evaluated measure of the oscillatory component produced by acoustic glitches is the second multiplet-frequency difference with respect to order n amongst modes of like degree l :

$$\Delta_2 \nu_{n,l} \equiv \nu_{n-1,l} - 2\nu_{n,l} + \nu_{n+1,l} \quad (6)$$

(Gough 1990). Any localized region of rapid variation

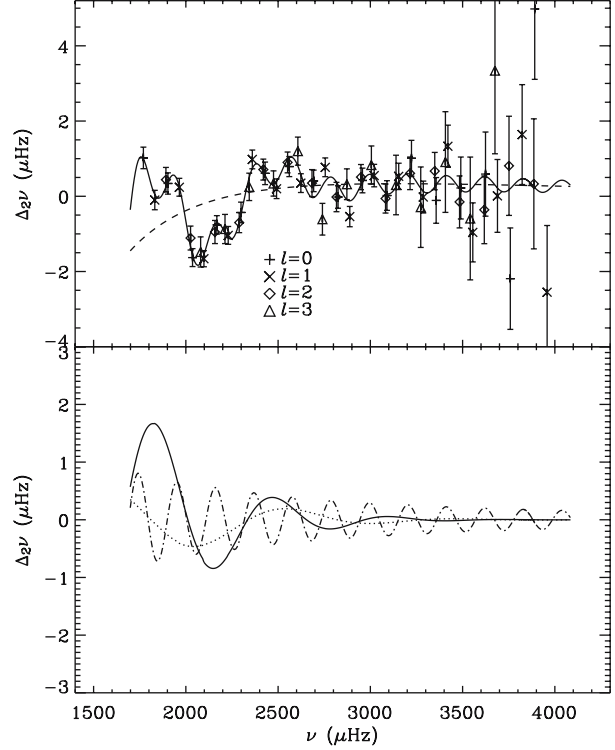


FIGURE 4. The symbols in the **upper panel** show second differences $\Delta_2 \nu_{n,l}$ (see equation 6) for low-degree ($l = 0, \dots, 3$) modes obtained from simulated data for a $1 M_{\odot}$ model of age 5.54 Gy. The simulation was based on two periods of 4-months observations, separated by 1 year, with the SONG network (see Grundahl et al. 2007). The solid curve is a fit to $\Delta_2 \nu$ based on the analysis by Houdek & Gough (2007). The dashed curve is a smooth contribution, modelled as a third-order polynomial in ν^{-1} , which represents near-surface effects. The **lower panel** displays the remaining individual contributions from the acoustic glitches to $\Delta_2 \nu$: the dotted and solid curves show the contribution from the first and second stages of helium ionization and the dot-dashed curve is the contribution from the acoustic glitch at the base of the convective envelope.

of either the sound speed c or the density scale height, or a spatial derivative of them, induces an oscillatory component in $\Delta_2 \nu$ (from here on the subscripts n, l have been dropped for simplicity) with a ‘cyclic frequency’ approximately equal to twice the acoustic depth

$$\tau = \int_{r_{\text{glitch}}}^R c^{-1} dr \quad (7)$$

of the glitch, and with an amplitude which depends on the amplitude of the glitch and which decays with ν once the inverse radial wavenumber of the mode becomes comparable with or less than the radial extent of the glitch.

Various approximate formulae for the oscillatory components that are associated with the helium ionization

have been suggested and used, by e.g., Basu et al. (1994, 2004), Monteiro & Thompson (1998, 2005) and Gough (2002), not all of which are derived directly from explicit acoustic glitches. Gough used an analytic function for modelling the dip in the first adiabatic exponent. In contrast, Monteiro & Thompson assumed a triangular form. Basu et al. have adopted a seismic signature for helium ionization that is similar to that arising from a single discontinuity; the artificial discontinuities in the sound speed and its derivatives that this and the triangular representations possess cause the amplitude of the oscillatory signal to decay with frequency too gradually, although that deficiency may not be immediately noticeable within the limited frequency range in which adequate asteroseismic data are or will imminently be available. More recently Houdek & Gough (2007) proposed a seismic diagnostic in which the variation of γ in the helium ionization zone is represented with a pair of Gaussian functions. This correctly results in a decay of the amplitude of the seismic signature with oscillation frequency that is faster than that which the triangular and the single-discontinuity approximations imply, and also takes some account of the two ionization states of helium. Moreover, they incorporated the acoustic cutoff frequency into the variation of the eigenfunction phase with acoustic depth, thereby improving the discrepancy between the seismically inferred depths of the acoustic glitches and that of a corresponding stellar model. An example of the application of Houdek & Gough's technique is presented in Fig. 4, which shows the resulting fit to simulated data for a solar-like star.

Mode parameters

Were solar p modes to be genuinely linear and stable, their power spectrum could be described in terms of an ensemble of intrinsically damped, stochastically driven, simple-harmonic oscillators, provided that the background equilibrium state of the star is independent of time (Fig. 5); if we assume further that mode phase fluctuations contribute negligibly to the width of the spectral lines, the intrinsic damping rates of the modes, $\Gamma/2$, could then be determined observationally from measurements of the pulsation linewidths Γ .

The power (spectral density), P , of the surface displacement $\xi_{nl}(t)$ of a damped, stochastically driven, simple-harmonic oscillator, satisfying

$$I_{nl} \left[\frac{d^2 \xi_{nl}}{dt^2} + \Gamma_{nl} \frac{d \xi_{nl}}{dt} + \omega_{nl}^2 \xi_{nl} \right] = f(t), \quad (8)$$

which represents the pulsation mode of order n and degree l , with linewidth Γ_{nl} and frequency ω_{nl} and mode inertia I_{nl} , satisfies

$$P \propto P_L P_f = \frac{\Gamma_{nl}/2\pi}{(\omega - \omega_{nl})^2 + \Gamma_{nl}^2/4} P_f, \quad (9)$$

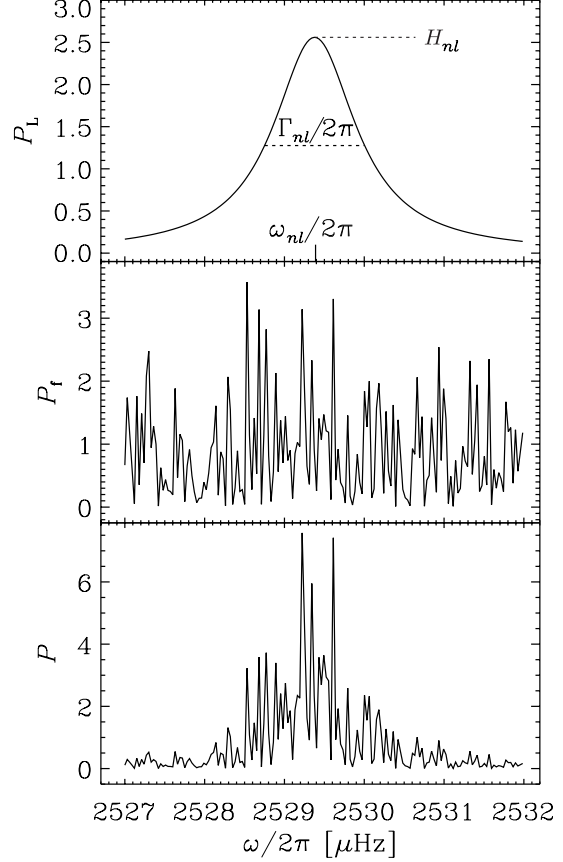


FIGURE 5. Power spectral density of a randomly excited, damped, harmonic oscillator. P_f represents the spectral density of the random force and P is the product of the Lorentzian P_L and P_f (adapted from Kosovichev 1995).

assuming $\Gamma_{nl} \ll \omega_{nl}$, where $f(t)$ describes the stochastic forcing function. Integrating equation (9) over frequency leads to the total mean energy in the mode

$$\begin{aligned} I_{nl} V_{nl}^2 &:= \frac{1}{2} \omega_{nl}^2 I_{nl} \langle |A_{nl}|^2 \rangle \propto \omega_{nl}^2 I_{nl} \int_{-\infty}^{\infty} P(\omega) d\omega \\ &\propto \frac{P_f(\omega_{nl})}{\Gamma_{nl}}, \end{aligned} \quad (10)$$

where A_{nl} is the displacement amplitude (angular brackets, $\langle \rangle$, denote an expectation value) and $V_{n,l}$ is the rms velocity of the displacement. The total mean energy of a mode is therefore directly proportional to the rate of work (also called energy supply rate) of the stochastic forcing P_f at the frequency ω_{nl} and indirectly proportional to Γ_{nl} .

Equations (8)–(10) are discussed in terms of the displacement ξ (from here on we omit the subscripts n and l), but in order to have a direct relation between the observed velocity signal $v(t) = d\xi/dt$ and the modelled excitation rate P_f we shall first take the Fourier transform $\tilde{V}(v)$ of $v(t)$ ($v = \omega/2\pi$). It follows that the total mean

energy E of the harmonic signal of a single pulsation mode is then given by (Chaplin et al. 2005)

$$E = IV^2 = I\hat{\delta} \int_{-\infty}^{\infty} |\tilde{V}(v)|^2 dv = \frac{1}{4}I\Gamma H, \quad (11)$$

in which

$$H := \int_{v-\hat{\delta}/2}^{v+\hat{\delta}/2} |\tilde{V}(v)|^2 dv, \quad (12)$$

is the maximum power density - which corresponds to the ‘height’ of the resonant peak in the frequency domain (see Fig. 2). The height H is the maximum of the discrete power, i.e. the integral of power spectral density over a frequency bin $\hat{\delta} = 1/T_{\text{obs}}$, where T_{obs} is the total observing time. The following expressions

$$V^2 := \frac{P_f}{\Gamma I} = \frac{1}{4}\Gamma H \quad (13)$$

and

$$H := \frac{P_f}{(\Gamma/2)^2 I} \quad (14)$$

provide a direct relation between the observed height H (in $\text{cm}^2 \text{s}^{-2} \text{Hz}^{-1}$), the modelled energy supply rate P_f (in erg s^{-1}), and damping rate $\eta = \Gamma/2$.

PULSATION COMPUTATIONS AND AMPLITUDE RATIOS

The linearized pulsation equations for nonadiabatic radial oscillations can be presented as (e.g. Balmforth 1992a):

$$\begin{aligned} \frac{\partial}{\partial m} \left(\frac{\delta p}{p} \right) &= \hat{f} \left(\frac{\delta r}{r}, \frac{\delta T}{T}, \frac{\delta p}{p}, \frac{\delta p_t}{p}, \frac{\delta \Phi}{\Phi} \right), \\ \frac{\partial}{\partial m} \left(\frac{\delta r}{r} \right) &= -\frac{1}{4\pi r^3 \rho} \left(3 \frac{\delta r}{r} + \frac{\delta \rho}{\rho} \right), \\ \frac{\partial}{\partial m} \left(\frac{\delta L}{L} \right) &= -i\omega \frac{c_p T}{L} \left(\frac{\delta T}{T} - \nabla_{\text{ad}} \frac{\delta p}{p} \right), \end{aligned} \quad (15)$$

where δ is the Lagrangian perturbation operator, and for simplicity the right hand side of the perturbed momentum equation is formally expressed by the function \hat{f} (the full set of equations can be found in, e.g., Balmforth 1992a). Equations (15) are solved subject to boundary conditions to obtain the eigenfunctions and the complex angular eigenfrequency $\omega = \omega_r + i\eta$, where ω_r is the (real) pulsation frequency and $\eta = \Gamma/2$ is the damping rate in (s^{-1}). The turbulent flux perturbations of heat and momentum, δL_c and δp_t , and the fluctuating anisotropy factor $\delta \Phi$ are obtained from the non-local, time-dependent convection formulation by Gough (1977a,b).

From the linearized nonadiabatic pulsation equations (15) theoretical intensity-velocity amplitude ratios

$$\frac{\Delta L_s}{\Delta V} := \frac{\delta L/L}{\omega_r \delta r/r} \quad (16)$$

TABLE 1. Absorption lines and their wavelengths λ of various helioseismic instruments. Also listed are the optical depths τ_{5000} at 5000 Å and the corresponding approximate heights above the photosphere ($h = 0$ at $T = T_{\text{eff}}$) at which the lines are formed.

Instrument	line	λ (Å)	τ_{5000}	height (km)
BBSO	Ca	6439	0.05	$\sim 129^*$
BiSON	K	7699	0.013	$\sim 250^\dagger$
MDI	Ni I	6708	9×10^{-3}	$\sim 300^{**}$
GOLF	Na D1/D2	5690	5×10^{-4}	$\sim 500^{**}$

* from Libbrecht (1988)

† from Christen-Dalsgaard & Gough (1982)

** from Toutain et al. (1997, but see also Baudin et al. 2005)

can be compared with observations, without the need of a specific excitation model and all its uncertainties in describing the turbulent spectra.

It is, however, important to realize that various instruments observe in different absorption lines and consequently at different heights in the atmosphere. This property has to be taken into account not only when comparing observations between various instruments (e.g. Christensen-Dalsgaard & Gough 1982), but also when comparing theoretical amplitude estimates with observations (Houdek et al. 1995). Table 1 lists some of the relevant properties of various instruments.

In the top panel of Fig. 6 the theoretical amplitude ratios (equation (16)) of a solar model are plotted as a function of height for several radial pulsation modes. The mode energy density (which is proportional to $rp^{1/2}\delta r$) increases rather slowly with height; the density ρ , however, decreases very rapidly and consequently the displacement eigenfunction δr increases with height. This leads to the results shown in the upper panel of Fig. 6 where the decrease in the amplitude ratios with height is particularly pronounced for high-order modes for which the eigenfunctions vary rapidly in the evanescent outer layers of the atmosphere. It is for that reason why solar velocity amplitudes from, e.g., the GOLF instrument have larger values than the measurements from the BiSON instrument (by about 25%, Kjeldsen et al. 2005). The lower panel of Fig. 6 compares the estimated solar amplitude ratios (curves) with observed ratios (symbols) as a function of frequency. The model results are depicted for velocity amplitudes computed at different atmospheric levels. The observations are obtained from accurate irradiance measurements from the IPHIR instrument of the PHOBOS 2 spacecraft with contemporaneous low-degree velocity data from the BiSON instrument at Tenerife (Schrijver et al. 1991). The thick solid curve represents a running-mean average, with a width of 300 μHz , of the observational data. The theoretical ratios

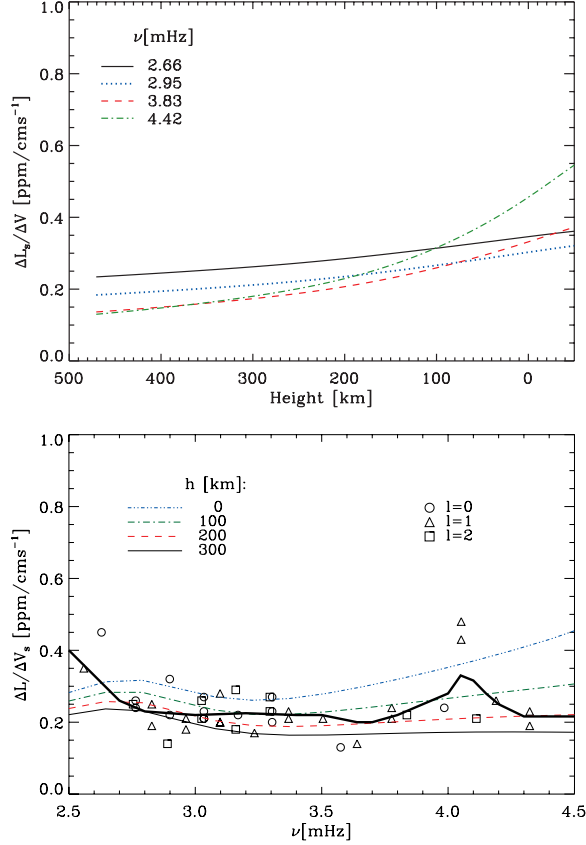


FIGURE 6. **Top:** Calculated amplitude ratios (see equation (16)) as a function of height in a solar model for modes with different frequency values. **Bottom:** Theoretical amplitude ratios (surface luminosity perturbation over velocity) for a solar model compared with observations by Schrijver et al. (1991). Computed results are depicted at different heights above the photosphere ($h=0$ km at $T = T_{\text{eff}}$). The thick, solid curve indicates a running-mean average of the data (from Houdek et al. 1995).

for $h = 200$ km (dashed curve) show reasonable agreement with the observations.

In Fig. 7 model results for the F5 star Procyon A are compared with observations (horizontal dotted line) by Arentoft et al. (2008). Theoretical results are shown for two stellar atmospheres: a VAL-C (Vernazza et al. 1981) atmosphere scaled with the model’s effective temperature T_{eff} (thin curves), and for an Eddington atmosphere (thick curves). For both stellar atmospheres the agreement with the observations is less satisfactory than in the solar case, indicating that we may not represent correctly the shape of the pulsation eigenfunctions. Consequently there is need for adopting more realistically computed atmospheres in the equilibrium models, particularly for stars with much higher surface temperatures than the Sun. It should, however, be mentioned that the current photometric observations are still uncertain.

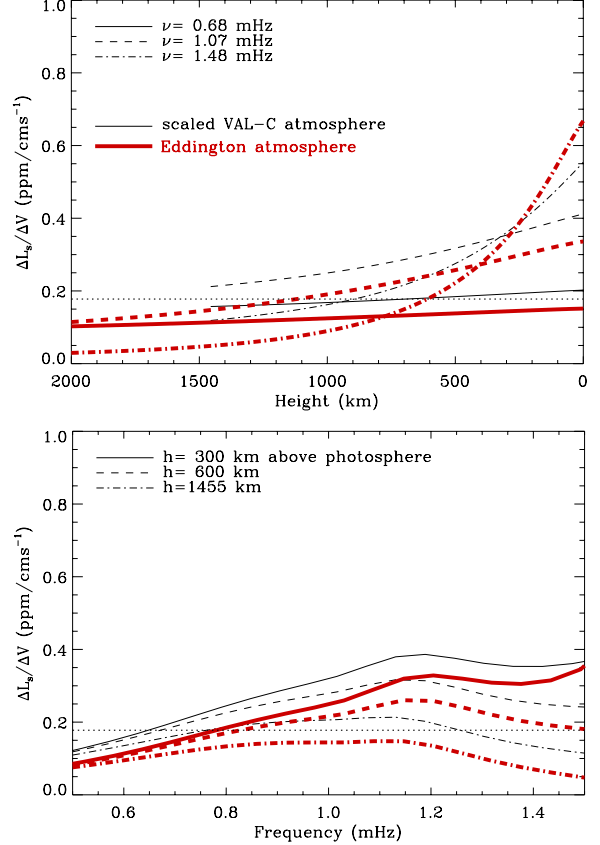


FIGURE 7. Calculated amplitude ratios (see equation (16)) for a model of Procyon A are compared with observations by Arentoft et al. (2008; horizontal dotted line). Theoretical results are shown for a scaled VAL-C atmosphere (black, thin curves) and for an Eddington atmosphere (red, thick curves). **Top:** The theoretical amplitude ratios are shown as a function of height and for three different pulsation modes. The frequencies of the three pulsation modes are indicated. **Bottom:** The theoretical amplitude ratios are shown as a function of frequency at three different heights in the stellar atmosphere. The heights above the photosphere $h = 0$ km are indicated.

DAMPING RATES

Damping of stellar oscillations arises basically from two sources: processes influencing the momentum balance, and processes influencing the thermal energy equation. Each of these contributions can be divided further according to their physical origin, which was discussed in detail by Houdek et al. (1999).

Important processes that influence the thermal energy balance are nonadiabatic processes attributed to the modulation of the convective heat flux by the pulsation. This contribution is related to the way that convection modulates large-scale temperature perturbations induced by the pulsations which, together with the conventional κ -mechanism, influences pulsational stability.

Current models suggest that an important contribution

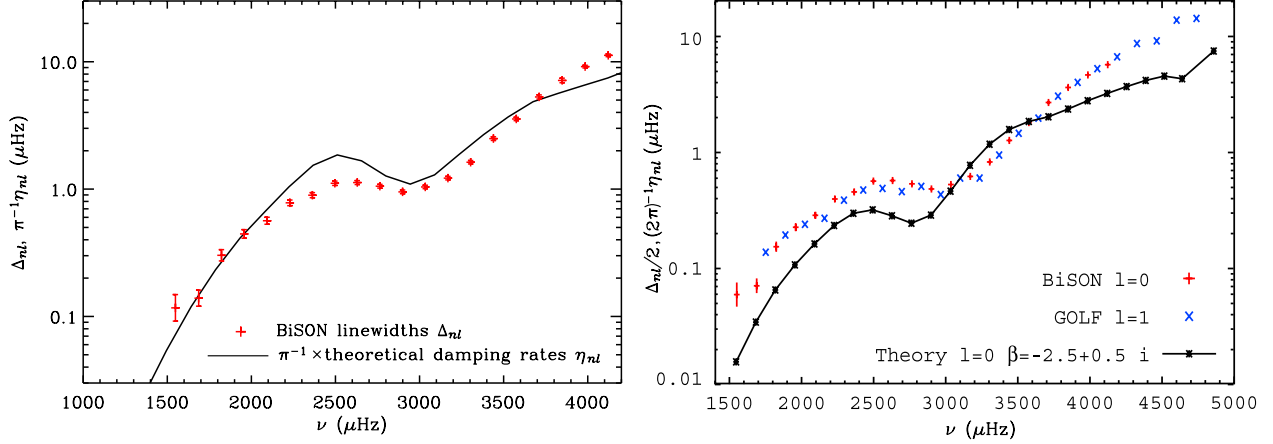


FIGURE 8. The symbols in the left-hand panel are the measured linewidths $\Delta_{nl} = \Gamma_{nl}/2\pi$ (we denote the FWHM in unit of cyclic frequency by Δ_{nl}) of solar low-degree p modes obtained from a 3456-d data set collected by BiSON between 1991 and 2000 (Chaplin et al. 2005). The data are compared with the theoretical damping rates $\pi^{-1}\eta_{nl}$ (connected by the solid curve) obtained from the model computations discussed in the previous section (from Chaplin et al. 2005). In the right-hand panel theoretical results of $(2\pi)^{-1}\eta_{nl}$ (solid curve) by Dupret et al. (2004) are compared with observations of $\Delta_{nl}/2$ (symbols).

that influences the momentum balance is the exchange of energy between the pulsation and the turbulent velocity field through dynamical effects of the fluctuating Reynolds stress. In fact, it is the modulation of the turbulent fluxes by the pulsations that seems to be the predominant mechanism responsible for the driving and damping of solar-type acoustic modes. It was first reported by Gough (1980) that the dynamical effects arising from the turbulent momentum flux perturbation δp_t contribute significantly to the damping Γ . Detailed analyses (Balmforth 1992a) reveal how damping is controlled largely by the phase difference between the momentum perturbation and the density perturbation. Therefore, turbulent pressure fluctuations must not be neglected in stability analyses of solar-type p modes.

A comparison between the latest linewidth measurements (full-width at half-maximum) $\Delta_{nl} = \Gamma_{nl}/2\pi$ and theoretical damping rates is given in Fig. 8. The observational time series from BiSON (Chaplin et al. 2005) was obtained from a 3456-d data set and the linewidths of the temporal power spectrum extend over many frequency bins $\delta\hat{\nu} = 1/2T_{\text{obs}}$. In that case the linewidth in units of cyclic frequency is related to the damping rate according to

$$\Delta_{nl} = \pi^{-1}\eta_{nl}. \quad (17)$$

Recently Dupret et al. (2004) performed similar stability computations for the Sun using the time-dependent mixing-length formulation by Gabriel et al. (1975, 1998) and Grigahcène et al. (2005), which is based on the formulation by Unno (1967). Their results are illustrated in the right panel of Fig. 8, which also shows the characteristic plateau near 2.8 mHz. It is, however, interesting to note that their findings suggest the fluctuating convective

heat flux to be the main contribution to mode damping, whereas for the model results shown in the left panel of Fig. 8, which are based on Gough’s (1977a,b) convection formulation, it is predominantly the fluctuating Reynolds stress that makes all modes stable.

Houdek et al. (1999) computed damping rates η of solar-like oscillations in about 160 stars with masses between $0.9M_{\odot}$ and $2.0M_{\odot}$ in the vicinity of the main sequence, and for various metallicities and convection parameters. Recently Chaplin et al. (2009) conducted a similar theoretical study of estimating mode lifetimes $\tau = \eta^{-1}$ in low-mass stars and compared the theoretical estimates with the latest linewidth measurements in twelve solar-type variables. They found that the mean mode lifetimes of the five most prominent solar-like p modes $\langle\tau\rangle$ scale like

$$\langle\tau\rangle \propto T_{\text{eff}}^{-4}. \quad (18)$$

Their results are depicted in Fig. 9, where the diamond symbols are the theoretical estimates of $\langle\tau\rangle$ obtained from a grid of models computed in the manner of Chaplin et al. (2005) and the crosses with error bars are the linewidth measurements of twelve main-sequence, sub-giant and red-giant stars.

STOCHASTIC EXCITATION

Because of the lack of a complete model for convection, the mixing-length formalism still represents the main method for computing the turbulent fluxes in the convectively unstable layers in a star. One of the assumptions in the mixing-length formulation is the Boussinesq approximation, which results in neglecting the acoustic wave generation by assuming the fluid to be incompressible.

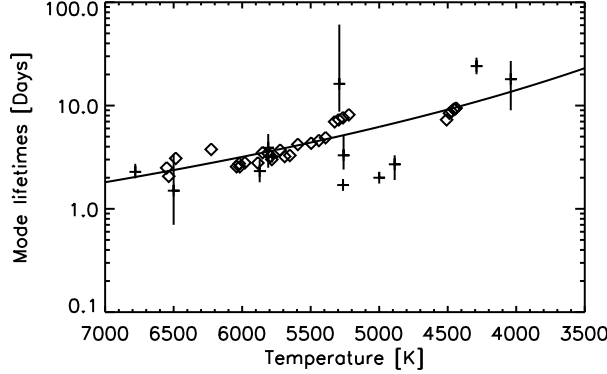


FIGURE 9. Average mode lifetimes $\langle \tau \rangle$ (averaged over the five most prominent p modes) in low-mass stars. The diamond symbols are the results from the stellar equilibrium and pulsation calculations and the cross symbols are observations of 12 main-sequence, sub-giant and red-giant stars. The solid curve represents the power law T_{eff}^{-4} , where T_{eff} is the surface temperature of the models that were used in the stability computations (from Chaplin et al. 2009).

Consequently a separate model is needed to estimate the rate of the acoustic noise (energy supply rate) generated by the turbulence. The excitation process can be regarded as multipole acoustic radiation (Lighthill 1952). Acoustic radiation by turbulent multipole sources in the context of stellar aerodynamics has been considered by Unno & Kato (1962), Moore & Spiegel (1964), Unno (1964), Stein (1967), Goldreich & Keeley (1977), Bohn (1984), Osaki (1990), Goldreich & Kumar (1990), Balmforth (1992b), Goldreich, Murray & Kumar (1994), Musielak et al. (1994), Samadi & Goupil (2001) and Chaplin et al. (2005).

The mean amplitude A of a mode is determined by a balance by the energy supply rate P_f from the turbulent velocity field and the thermal and mechanical dissipation rate characterized by the damping coefficient η [see equation (10)]. The procedure that we adopt to estimate A is that of Chaplin et al. (2005), whose prescription follows that of Balmforth (1992b).

We represent the linearized pulsation dynamics by the simplified equation

$$\rho \left(\frac{\partial^2 \xi}{\partial t^2} + 2\eta \frac{\partial \xi}{\partial t} + \mathcal{L} \xi \right) = \mathbf{F}(\mathbf{u}) + \mathbf{G}(s') \quad (19)$$

for the displacement $\xi(\mathbf{r}, t)$, which is now also a function of radius \mathbf{r} , of a forced oscillation corresponding to a single radial mode satisfying the homogeneous equation

$$\mathcal{L} \xi(\mathbf{r}) = \omega^2 \xi(\mathbf{r}) \quad (20)$$

in which ω (and ξ) are real and \mathcal{L} is a linear spatial operator. The (inhomogeneous) fluctuating terms on the

right-hand-side of equation (19) arise from the fluctuating Reynolds stresses

$$\mathbf{F}(\mathbf{u}) = \nabla \cdot (\rho \mathbf{u} \mathbf{u} - \langle \rho \mathbf{u} \mathbf{u} \rangle) \quad (21)$$

and from the fluctuating gas pressure (due to the fluctuating buoyancy force), represented by $\mathbf{G}(s')$, where s' is the Eulerian entropy fluctuation (Bohn 1984; Osaki 1990; Goldreich & Kumar 1990; Balmforth 1992b; Goldreich, Murray & Kumar 1994; Samadi & Goupil 2001). The latest numerical simulations by Stein et al. (2004) suggest that both forcing terms in equation (19) contribute to the energy supply rate P_f by about the same amount, a result that was also reported by Samadi et al. (2003) using the turbulent velocity field and anisotropy factors from numerical simulations (Stein & Nordlund 2001). In this paper we consider only the term of the fluctuating Reynolds stresses and because we use only radial modes, only the vertical component F_3 of \mathbf{F} is important,

$$F_3(u_3) \simeq \frac{\partial}{\partial r} (\rho u_3^2 - \langle \rho u_3^2 \rangle). \quad (22)$$

If we define the vertical component of the velocity correlation as $R_{33} = \langle u_3 u_3 \rangle$, its Fourier transform \hat{R}_{33} can be expressed in the Boussinesq-quasi-normal approximation (e.g. Batchelor 1953) as a function of the turbulent energy spectrum function $E(k, \omega)$:

$$\hat{R}_{33} = \frac{\Psi E(k, \omega)}{12\pi k^2}, \quad (23)$$

where k is a wavenumber and Ψ is an anisotropy parameters given by

$$\Psi = [2\Phi/3(\Phi - 1)]^{1/2}, \quad (24)$$

which is unity for isotropic turbulence (Chaplin et al. 2005). This factor was neglected in previously published excitation models but it has to be included in a consistent computation of the acoustic energy supply rate. Following Stein (1967) we factorize the energy spectrum function into $E(k, \omega) = \tilde{E}(k) \Omega(\omega; \tau_k)$, where $\tau_k = \lambda / k u_k$ is the correlation time-scale of eddies of size π/k and velocity u_k ; the correlation factor λ is of order unity and accounts for uncertainties in defining τ_k .

The energy supply rate is then given by (see Chaplin et al. 2005 for details)

$$P_f = \frac{\pi}{9I} \int_0^R \ell^3 \left(\Phi \Psi r p_t \frac{\partial \xi_r}{\partial r} \right)^2 \mathcal{S}(r; \omega) dr, \quad (25)$$

with

$$\mathcal{S}(r; \omega) = \int_0^\infty \kappa^{-2} \tilde{E}^2(\kappa) \tilde{\Omega}(\tau_k; \omega) d\kappa, \quad (26)$$

where $\kappa = k\ell/\pi$, ℓ is the mixing length, R is surface radius, and ξ_r is the normalized radial part of ξ . The spectral function \mathcal{S} accounts for contributions to P_f from the

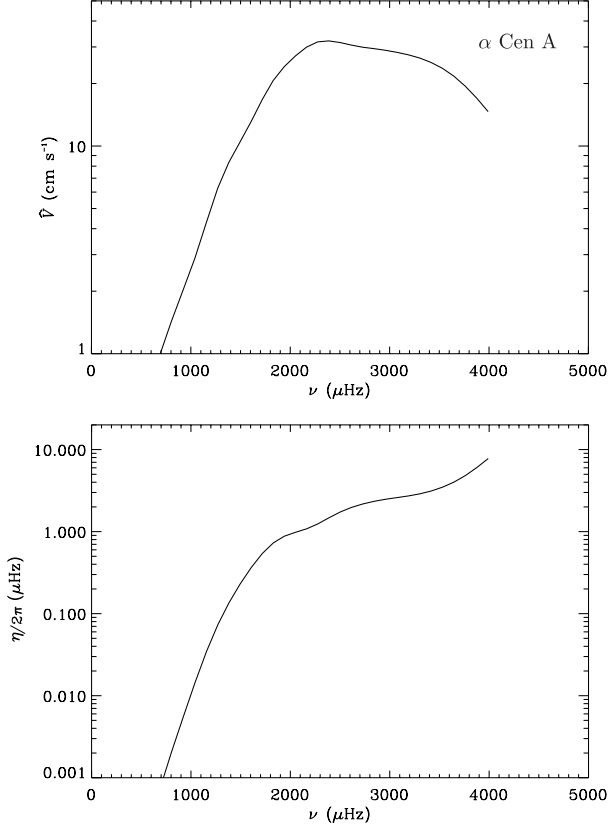


FIGURE 10. **Top:** Predicted apparent velocity amplitudes (defined to be $\sqrt{2}$ times the rms value) for a model of α Cen A, computed according to equation (13). **Bottom:** Linear damping rates for a model of α Cen A, obtained by solving the fully nonadiabatic pulsation equations (15).

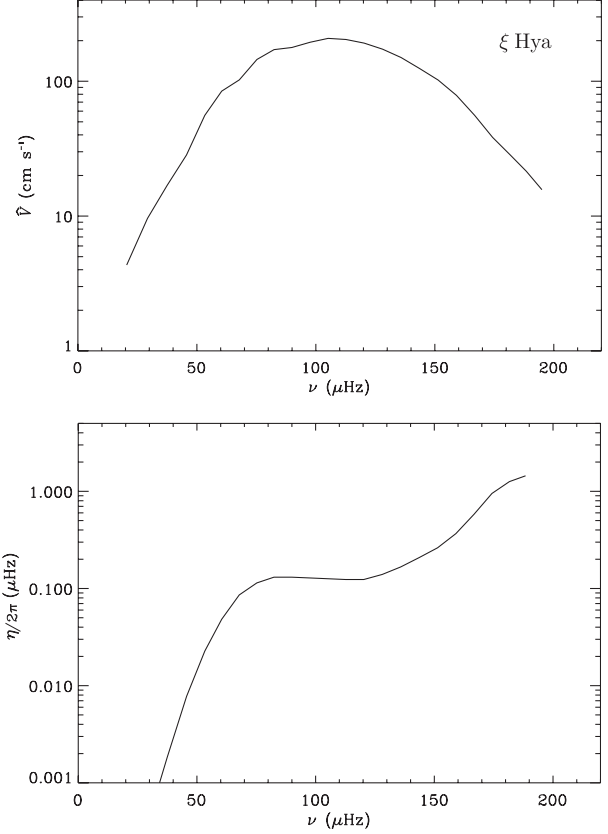


FIGURE 11. **Top:** Predicted apparent velocity amplitudes (defined to be $\sqrt{2}$ times the rms value) for a model of ξ Hydrae, computed according to equation (13). **Bottom:** Linear damping rates for a model of ξ Hydrae, obtained by solving the fully nonadiabatic pulsation equations (15) (adapted from Houdek & Gough 2002).

small-scale turbulence and includes the normalized spatial turbulent energy spectrum $\tilde{E}(k)$ and the frequency-dependent factor $\Omega(\tau_k; \omega)$. For $\tilde{E}(k)$ it has been common to adopt either the Kolmogorov (Kolmogorov 1941) or the Spiegel spectrum (Spiegel 1962). The frequency-dependent factor $\Omega(\tau_k; \omega)$ is still modelled in a very rudimentary way and we adopt two forms:

– the Gaussian factor (Stein 1967),

$$\Omega_G(\omega; \tau_k) = \frac{\tau_k}{\sqrt{2\pi}} e^{-(\omega\tau_k/\sqrt{2})^2}; \quad (27)$$

– the Lorentzian factor (Gough 1977b; Samadi et al. 2003; Chaplin et al. 2005),

$$\Omega_L(\omega; \tau_k) = \frac{\tau_k}{\pi\sqrt{2\ln 2}} \frac{1}{1 + (\omega\tau_k/\sqrt{2\ln 2})^2}. \quad (28)$$

The Lorentzian frequency factor is a result predicted for the largest, most-energetic eddies by the time-dependent mixing-length formulation of Gough (1977b). Recently, Samadi et al. (2003) reported that Stein & Nordlund’s

hydrodynamical simulations also suggest a Lorentzian frequency factor, which decays more slowly with depth z and frequency ω than the Gaussian factor. Consequently a substantial fraction to the integrand of equation (25) arises from eddies situated in the deeper layers of the Sun, resulting in a larger acoustic excitation rate P_f .

OSCILLATION AMPLITUDES

Model predictions of the mode height H were computed according to equation (14). As in the solar case damping rates for other stars are obtained from solving the eigenvalue problem (15) and the energy supply rates are calculated from expression (25). With these estimates for η and P_f Houdek & Gough (2002) predicted velocity amplitudes for several stars, using equation (13). Results for stochastically excited oscillation amplitudes and linear damping rates in the solar-like star α Cen A and in the sub-giant ξ Hydrae are illustrated in Figs 10 and 11. Kjeldsen et al. (2005) reported mode lifetimes for

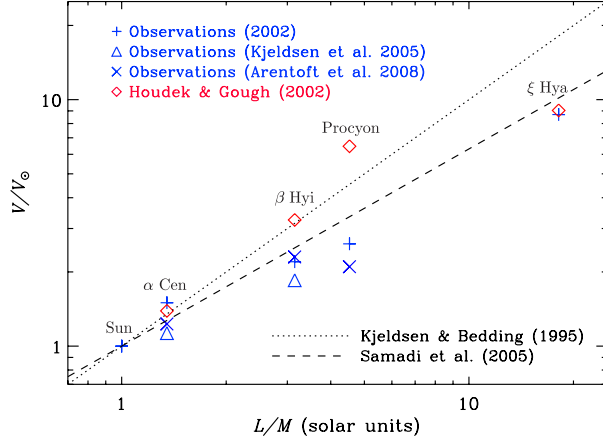


FIGURE 12. Predicted apparent velocity amplitudes (defined to be $\sqrt{2}$ times the rms value) as function of light-to-mass ratio for stochastically excited oscillations in other stars. Observations from several authors are plotted by the plus and triangle symbols. The theoretical estimates by Houdek & Gough (2002) are plotted as diamond symbols. The scaling law of Kjeldsen & Bedding (1995) is illustrated by the dotted line and results reported by Samadi et al. (2005) are indicated by the dashed line.

α Cen A of about 2.1 days (but see also Fletcher et al. 2006), which are in reasonable agreement with the theoretical estimates of about 1.7 days for the most prominent modes (the mode lifetime $\tau = \eta^{-1}$; see lower panel of Fig. 10). For ξ Hydrae, however, the theoretical mode lifetime of the most prominent modes is about 18 days which is in stark contrast to the measured value of about 2–3 days by Stello et al. (2004, 2006), yet the estimated velocity amplitudes for ξ Hydrae are in almost perfect agreement with the observations by Frandsen et al. (2002).

A comparison between predicted and observed velocity amplitudes in several solar-type pulsators is illustrated in Fig. 12. The dotted line is the scaling law by Kjeldsen & Bedding (1995), which is based on the computations by Christensen-Dalsgaard & Frandsen (1983), and the dashed line is the scaling relation reported by Samadi et al. (2005) using the convective velocity profiles from 3D numerical simulations (Stein & Nordlund 2001), a Lorentzian frequency factor in equation (26), and the theoretical damping rates from Houdek et al. (1999). For the cooler stars the theoretical results (scaling laws) are in reasonable agreement with the observations, whereas for hotter stars, such as for Procyon A, the theoretical velocity amplitudes are overestimated by both the scaling laws and the stochastic excitation models.

Recently, Chaplin et al. (2009) suggested a new scaling law for the intensity amplitudes by combining their finding of the mean mode lifetime, $\langle \tau \rangle \propto T_{\text{eff}}^{-4}$ [cf. equation (18)], with Kjeldsen & Bedding’s (1995) scaling law

for the intensity amplitudes inferred from a narrow-band observation of wavelength λ , i.e. $(\delta L/L)_\lambda \propto (L/M)/T_{\text{eff}}^2$, leading to

$$H \propto g^{-2} \quad (29)$$

for the maximum mode height. Since the surface gravity changes fairly slowly along the main sequence, the new scaling relation (29) for H , which assumes narrow-band intensity observations, suggests that stars notably cooler than the Sun might have mode heights that are comparable to those solar-like pulsators that are hotter than the Sun. Moreover, Hekker et al. (2009) reported that the intensity heights in about 780 red giant stars, observed in broadband photometry with the CoRoT satellite, follow the scaling law $H \propto g^{-2.2}$, a result that supports the theoretical finding (29) by Chaplin et al. 2009.

STELLAR-CYCLE EFFECTS

From helioseismic data, such as those provided by the BiSON, we have learnt that not only the oscillation frequencies change with time over the 11-year solar cycle but also the height H and width Γ . In the solar case the absolute fractional change from solar activity minimum to maximum in $\langle H \rangle$ (angular brackets $\langle \rangle$ denote an average over the five most prominent p modes) is about 40%. That in $\langle \Gamma \rangle$ is about 20% (Chaplin et al. 2000). We therefore expect also in solar-like oscillators not only the mode frequencies but also the mode heights and linewidths to show stellar-cycle variations.

Chaplin et al. (2007, 2008) estimated stellar-cycle frequency shifts and mode height variations for a grid of 31 models with masses between $0.7 M_\odot$ and $1.3 M_\odot$ and stellar ages, t_* , in the range from the ZAMS to 9 Gy, using the Padova isochrones (e.g., Bonatto et al. 2004) to specify mass, radius, effective temperature, T_{eff} , and luminosity. The evolutionary tracks of these models are presented in the left panel of Fig. 13 in terms of a (t_*, T_{eff}) plot. To predict the stellar-cycle changes Chaplin et al. used the Ca II H&K index for surface activity in stars. This index is usually expressed as R'_{HK} , the average fraction of the star’s total luminosity that is emitted in the H&K line cores. The authors then used the data of 22 main-sequence stars collected by the Mount Wilson Ca II H&K programme (e.g., Saar & Brandenburg 2002) from which the R'_{HK} cycle amplitude values, $\Delta R'_{\text{HK}}$, were determined. The $\Delta R'_{\text{HK}}$ values were then simply scaled against the $0.4 \mu\text{Hz}$ frequency shift seen for the most prominent low- l modes in the Sun, assuming that the frequency shifts $\delta \nu_{\text{cyc}}$ scale approximately linearly with $\Delta R'_{\text{HK}}$. In order to estimate the frequency shifts of the 31 grid models, it was necessary to calculate first the R'_{HK} values for the 31 models. This was done according to the procedure by Noyes (1983) and Noyes et al. (1984). The R'_{HK} values so obtained were then used to estimate the corresponding cycle frequency shifts by

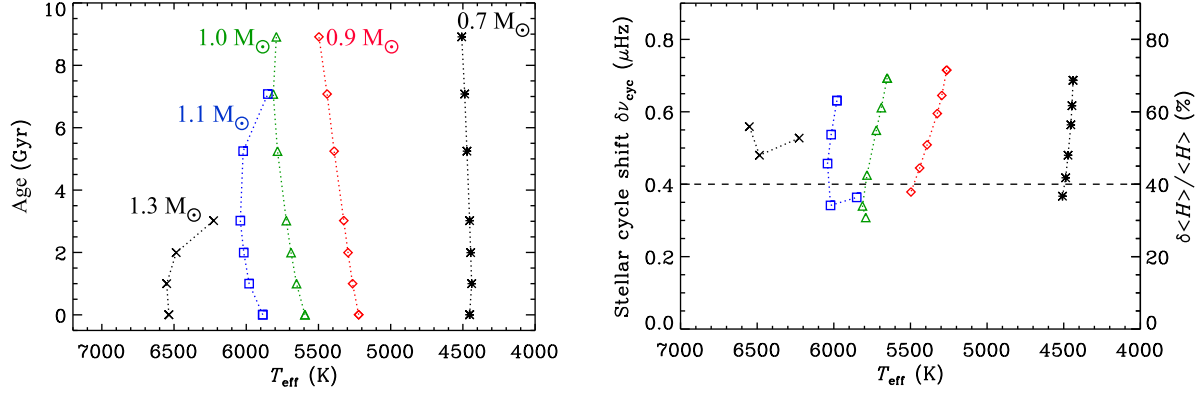


FIGURE 13. **Left:** Age – effective temperature plot for a sequence of stellar models, obtained from the Padova isochrones, for which the stellar-cycle induced frequency shifts and mode height variations were predicted. **Right:** Predicted stellar-cycle frequency shifts (left ordinate) and relative height variations (right ordinate) for a sequence of stellar models with masses between $0.7 M_{\odot}$ and $1.3 M_{\odot}$ (from Chaplin et al. 2008).

interpolating linearly in the $(\delta\nu_{\text{cyc}}, R'_{\text{HK}})$ table of the 22 main-sequence stars observed by the Mount Wilson Ca II H&K programme (for a detailed discussion see Chaplin et al. 2007). The outcome of this procedure for estimating the stellar-cycle frequency shifts of the most prominent p modes in the stellar models is depicted in the right panel (left ordinate) of Fig. 13. Also shown in this figure are the predicted fractional changes in $\langle H \rangle$ (right ordinate), obtained in a similar way as the frequency shifts and assuming a fractional change of $\langle H \rangle$ of 40% for the Sun. These results suggest that, in the considered age range of 1 – 9 Gy, the variation of p-mode frequencies and heights over the stellar cycle can be up to 1.5 – 2 times larger than in the Sun, and that these variations depend predominantly on stellar age and less on T_{eff} or stellar mass.

ACKNOWLEDGMENTS

I am grateful to Douglas Gough for helpful discussions. Support by the Austrian Science Fund (FWF project P21205) is gratefully acknowledged.

REFERENCES

1. Aerts C., Christensen-Dalsgaard J., Cunha M., Kurtz D. 2008, *Solar Phys.* 251, 3
2. Arentoft T., Kjeldsen H., Bedding T.R., Bazot M., Christensen-Dalsgaard J., Dall T.H., Karoff C., Carrier F. et al. 2008, *AJ* 687, 1180
3. Baglin A. 2003, *Advances Space Res.* 31, 345
4. Balmforth N.J. 1992a, *MNRAS* 255, 603
5. Balmforth N.J. 1992b, *MNRAS* 255, 639
6. Basri G.B., Borucki W.J., Koch D.G. 2005, *New Astronomy Rev.* 49, 478
7. Basu S., Antia H.M., Narasimha D. 1994, *MNRAS* 267, 209
8. Basu S., Mazumdar A., Antia H. M., Demarque P. 2004, *MNRAS* 350, 277
9. Batchelor G.K. 1953, *Homogeneous Turbulence*, Cambridge University Press, Cambridge
10. Baudin F., Samadi R., Goupil M.-J., Appourchaux T., Barban C., Boumier P., Chaplin W.J., Gouttebroze P. 2005, *A&A* 433, 349
11. Bedding T.R., Kjeldsen H. 2007, in: *Unsolved Problems in Stellar Physics*, eds Stancliffe R.J., Dewi J., Houdek G., Martin R.G., Tout C.A., AIP Conf. Proc. 948, p. 117
12. Bohn H.U. 1984, *A&A* 136, 338
13. Bonatto Ch., Bica E., Girardi L. 2004, *A&A* 415, 571
14. Brown, T.M., Gilliland, R.L., Noyes, R.W., Ramsey, L.W. 1991, *ApJ* 368, 599
15. Carrier, F., Bouchy, F., Eggenberger, P. 2003, in: *Asteroseismology Across the HR Diagram*, eds Thompson, M.J., Cunha, M.S., Monteiro, M.J.P.F.G., Kluwer, Dordrecht, 315
16. Chaplin W.J., Elsworth Y., Issak G.R., Miller B.A., New R. 2000, *MNRAS* 313, 32
17. Chaplin W., Houdek G., Elsworth Y., Gough D.O., Isaac G.R., New R. 2005, *MNRAS* 360, 859
18. Chaplin W.J., Elsworth Y., Houdek G., New R. 2007, *MNRAS* 377, 17
19. Chaplin W.J., Houdek G., Appourchaux T., Elsworth Y., New R., Toutain T. 2008, *A&A* 485, 813
20. Chaplin W.J., Houdek G., Karoff C., Elsworth Y., New R. 2009, *ApJ* 500, L21
21. Christensen-Dalsgaard J. 1993, in: *Proc. GONG 1992: Seismic investigation of the Sun and stars*, ed. T.M. Brown, ASP Conf. Ser. 42, San Francisco, p. 347
22. Christensen-Dalsgaard J. 2001, in: *Stellar Structure and Habitable Planet Finding*, eds Favata F., Roxburgh I. W., Galadi D., ESA SP-485, Noordwijk, p. 25
23. Christensen-Dalsgaard J. 2007, *CoAst* 150, 350
24. Christensen-Dalsgaard J., Gough D. 1982, *MNRAS* 198, 141
25. Christensen-Dalsgaard J., Frandsen S. 1983, *Solar Phys.* 82, 469
26. Dupret M.-A., Grigahcène A., Garrido R., Gabriel M., Noels A. 2004, in: *Proc. SOHO 14/GONG 2004 Workshop*, ed. D. Danesy, ESA SP-559, Noordwijk, p 207

27. Fletcher S.T., Chaplin W.J., Elsworth Y., Schou J., Buzasi D. 2006, MNRAS 371, 935
28. Frandsen S., Carrier F., Aerts C., et al. 2002, A&A 394, L5
29. Gabriel M., Scuflaire R., Noels A., Boury A. 1975, A&A 208, 122
30. Gabriel M. 1998, in: Proc. SOHO 6/GONG 98 Workshop, eds S. Korzennik, A. Wilson, ESA SP-418, Noordwijk, p. 863
31. Goldreich P., Keeley D.A. 1977, ApJ 212, 243
32. Goldreich P., Kumar P. 1990, ApJ 363, 694
33. Goldreich P., Murray N., Kumar P. 1994, ApJ 423, 466
34. Gough D.O. 1977a, in: Problems of stellar convection, eds E. Spiegel, J.-P. Zahn, Springer-Verlag, Berlin, p. 15
35. Gough D.O. 1977b, ApJ 214, 196
36. Gough D.O. 1980, in: Nonradial and Nonlinear Stellar Pulsation, eds H.A. Hill, W.A. Dziembowski, Springer-Verlag, Berlin, p. 273
37. Gough D.O. 1985, in: Proc. Future Missions in Solar, Heliospheric and Space Plasma Physics, eds E. Rolfe, B. Battirck, ESA SP-235, Noordwijk, p. 183
38. Gough D.O. 1986, in: Proc. Hydrodynamic and magnetohydrodynamic problems in the Sun and stars, ed. Y. Osaki, University of Tokyo, Tokyo, p. 117
39. Gough D. O. 1990, in: Progress of Seismology of the Sun and Stars, Lecture Notes in Physics, Vol. 367, eds Y. Osaki, H. Shibahashi, Springer Verlag, Berlin, p. 283.
40. Gough D. O. 1993, in: Astrophysical fluid dynamics, eds Zahn J.-P., Zinn-Justin J., Amsterdam, Elsevier, p. 399.
41. Gough D. O. 2001, in: Astrophysical Ages and Timescales, eds von Hippel T., Simpson C., Manset N., ASP Conf. Ser. Vol. 245, San Francisco, p. 31
42. Gough D. O. 2002, in: Stellar structure and habitable planet finding, eds Favata F., Roxburgh I. W., Galadi D., ESA SP-485, Noordwijk, p.65
43. Grigahcène A., Dupret M.-A., Gabriel M., et al. 2005, A&A 434, 1055
44. Grundahl F., Kjeldsen H., Christensen-Dalsgaard J., Arentoft T., Frandsen S. 2007, CoAst 150, 300
45. Hekker S., Kallinger T., Baudin F., De Ridder J., Barban C., Carrier F., Hatzes A.P., Weiss W.W., Baglin A. 2009, A&A 506, 465
46. Houdek G., Balmforth N., Christensen-Dalsgaard J. 1995, in: Proc. 4th SOHO Workshop, eds J.T. Hoeksema, V. Domingo, B. Fleck, B. Battirck, ESA SP-376, Vol. 2, Noordwijk, p. 447
47. Houdek G., Balmforth N.J., Christensen-Dalsgaard J., Gough D.O. 1999, A&A 351, 582
48. Houdek G., Gough D.O. 2002, MNRAS 336, L65
49. Houdek G., Gough D.O. 2007, MNRAS 375, 861
50. Houdek G., Gough D.O. 2008, in: The Art of Modelling Stars in the 21st Century, Deng, L., Chan, K. L., Chiosi C., eds IAU Symp., Vol. 252, CUP, Cambridge, p. 149
51. Kjeldsen H., Bedding T.R. 1995, A&A 293, 87
52. Kjeldsen H., Bedding T.R., Viskum M., Frandsen S. 1995, AJ 109, 1313
53. Kjeldsen H., Bedding T.R., Baldry I.K., Bruntt H., Butler R.P., Fischer D.A., Frandsen S., Gates E.L., Grundahl F., Lang K., Marcy G.W., Misch A., Vogt S.S. 2003 AJ 126, 1483
54. Kjeldsen H., Bedding T.R., Butler R.P., et al. 2005, ApJ 635, 1281
55. Kolmogorov A.N. 1941, Dokl. Akad. Nauk SSSR, 30, 299
56. Kosovichev A.G. 1995, in: Proc. of Fourth SOHO Workshop, eds J.T. Hoeksma, V. Domingo, B. Fleck, ESA SP-376, vol.2, Noordwijk, p. 165
57. Libbrecht K.G. 1988, ApJ 334, 510
58. Lighthill M.J. 1952, Proc. Roy. Soc. London A211, 564
59. Martić M., Schmitt J., Lebrun J.-C., Barban C., Connes P., Bouchy F., Michel E., Baglin A., Appourchaux T., Bertaux J.-L. 1999, A&A 351, 993
60. Monteiro M.J.P.F.G., Thompson M. J., 1998, in: Proc. IAU Symp. 185, New Eyes to see inside the Sun and Stars, eds Deubner F.-L., Christensen-Dalsgaard J., Kurtz D. W., Kluwer, Dordrecht, p. 317
61. Monteiro M. J. P. F. G., Thompson M. J. 2005, MNRAS 361, 1187
62. Musielak Z.E., Rosner R., Stein R.F., Ulmschneider P. 1994, ApJ 423, 474
63. Moore D.W., Spiegel E.A. 1964, ApJ 139, 48
64. Mosser B., Bouchy F., Martić M., Appourchaux T., Barban C., Berthomieu G., Garcia R.A., Lebrun J.C., Michel E., Provost J., Thévenin F., Turck-Chièze S. 2008, A&A 478, 197
65. Noyes R.W. 1983, in: Solar and Stellar Magnetic Fields, IAU Symp. 102, p 133
66. Noyes R.W., Hartmann L.W., Baliunas S.L., Duncan D.K., Vaughan A.H. 1984, ApJ 279, 763
67. Osaki Y. 1990, in: Progress of Seismology of the Sun and Stars, eds Y. Osaki Y., H. Shibahashi, Springer-Verlag, Berlin, p. 145
68. Saar S.H., Brandenburg A. 2002, Astron. Nachr. 323, 357
69. Samadi R., Goupil M.-J. 2001, A&A 370, 136
70. Samadi R., Nordlund Å., Stein R.F., Goupil M.-J., Roxburgh I., 2003, A&A 404, 1129
71. Samadi R., Goupil M.-J., Alecian E., et al. 2005, Journal of Astrophysics and Astronomy 26, 171
72. Schrijver C.J., Jiménez A., Däppen W. 1991, A&A 251, 655
73. Spiegel E. 1962, J. Geophys. Res. 67, 3063
74. Stein R.F. 1967, Solar Phys. 2, 385
75. Stein R.F., Nordlund Å. 2001, ApJ 546, 585
76. Stein R., Georgobani D., Trampedach R., Ludwig H.-G., Nordlund Å. 2004, Solar Phys. 220, 229
77. Stello D., Kjeldsen H., Bedding T.R., et al. 2004, Solar Phys. 200, 207
78. Stello D., Kjeldsen H., Bedding T.R., Buzasi D. 2006, A&A 448, 709
79. Tassoul M. 1980, ApJS 43, 469
80. Toutain T., Appourchaux T., Baudin F., et al. 1997, Solar Phys. 172, 311
81. Unno W. 1964, Trans. Int. astr. Un. XII(B), 555
82. Unno W. 1967, PASJ 19, 140
83. Unno W., Kato S. 1962, PASJ 14, 416
84. Vandakurov Y.V. 1967, Astron. Zh. 44, 786 (English translation: Sov. Astron. AJ 11, 630)
85. Vernazza J.E., Avrett E.H., Loeser R. 1981, ApJS 45, 635